

A MULTI-SITE CAMPAIGN TO MEASURE SOLAR-LIKE OSCILLATIONS IN PROCYON. I. OBSERVATIONS, DATA REDUCTION AND SLOW VARIATIONS

TORBEN ARENTOFT,¹ HANS KJELDSSEN,¹ TIMOTHY R. BEDDING,²
MICHAËL BAZOT,^{1,3} JØRGEN CHRISTENSEN-DALSGAARD,¹ THOMAS H. DALL,⁴ CHRISTOFFER KAROFF,¹
FABIEN CARRIER,⁵ PATRICK EGGENBERGER,⁶ DANUTA SOSNOWSKA,⁷
ROBERT A. WITTENMYER,⁸ MICHAEL ENDL,⁸ TRAVIS S. METCALFE,⁹
SASKIA HEKKER,^{10,11} SABINE REFFERT,¹²
R. PAUL BUTLER,¹³ HANS BRUNTT,² LÁSZLÓ L. KISS,² SIMON J. O'TOOLE,¹⁴
EJI KAMBE,¹⁵ HIROYASU ANDO,¹⁶ HIDEYUKI IZUMIURA,¹⁵ BUN'EI SATO,¹⁷
MICHAEL HARTMANN,¹⁸ ARTIE HATZES,¹⁸
FRANCOIS BOUCHY,¹⁹ BENOIT MOSSE,²⁰ THIERRY APPOURCHAUX,²¹ CAROLINE BARBAN,²⁰ GABRIELLE BERTHOMIEU,²²
RAFAEL A. GARCIA,²³ ERIC MICHEL,²⁰ JANINE PROVOST,²² SYLVAIN TURCK-CHIÈZE,²³
MILENA MARTIĆ,²⁴ JEAN-CLAUDE LEBRUN,²⁴ JEROME SCHMITT,²⁵ JEAN-LOUP BERTAUX,²⁴
ALFIO BONANNO,²⁶ SERENA BENATTI,²⁷ RICCARDO U. CLAUDI,²⁷ ROSARIO COSENTINO,²⁶ SILVIO LECCIA,²⁸
SØREN FRANDSEN,¹ KARSTEN BROGAARD,¹ LARS GLOWIENKA,¹ FRANK GRUNDAHL¹ AND ERIC STEMPELS²⁹

to appear in *ApJ*

ABSTRACT

We have carried out a multi-site campaign to measure oscillations in the F5 star Procyon A. We obtained high-precision velocity observations over more than three weeks with eleven telescopes, with almost continuous coverage for the central ten days. This represents the most extensive campaign so far organized on any solar-type oscillator. We describe in detail the methods we used for processing and combining the data. These involved calculating weights for the velocity time series from the measurement uncertainties and adjusting them in order to minimize the noise level of the combined data. The time series of velocities for Procyon shows the clear signature of oscillations, with a plateau of excess power that is centred at 0.9 mHz and is broader than has been seen for other stars. The mean amplitude of the radial modes is $38.1 \pm 1.3 \text{ cm s}^{-1}$ (2.0 times solar), which is consistent with previous detections from the ground and by the WIRE spacecraft, and also with the upper limit set by the MOST spacecraft. The variation of the amplitude during the observing campaign allows us to estimate the mode lifetime to be $1.5^{+1.9}_{-0.8} \text{ d}$. We also find a slow variation in the radial velocity of Procyon, with good agreement between different telescopes. These variations are remarkably similar to those seen in the Sun, and we interpret them as being due to rotational modulation from active regions on the stellar surface. The variations appear to have a period of about 10 days, which presumably equals the stellar rotation period or, perhaps, half of it. The amount of power in these slow variations indicates that the fractional area of Procyon covered by active regions is slightly higher than for the Sun.

Subject headings: stars: individual (Procyon A) — stars: oscillations

¹ Danish AsteroSeismology Centre (DASC), Department of Physics and Astronomy, University of Aarhus, DK-8000 Aarhus C, Denmark; toar@phys.au.dk, hans@phys.au.dk, jcd@phys.au.dk, karoff@phys.au.dk, srf@phys.au.dk, kfb@phys.au.dk, f002769@phys.au.dk, fgj@phys.au.dk

² Institute of Astronomy, School of Physics, University of Sydney, NSW 2006, Australia; bedding@physics.usyd.edu.au, bruntt@physics.usyd.edu.au, laszlo@physics.usyd.edu.au

³ Centro de Astrofísica da Universidade do Porto, Rua das Estrelas, 4150-762 Porto, Portugal; bazot@astro.up.pt

⁴ Gemini Observatory, 670 N. A'ohoku Pl., Hilo, HI 96720, USA; tdall@gemini.edu

⁵ Instituut voor Sterrenkunde, Katholieke Universiteit Leuven, Celestijnenlaan 200 B, 3001 Leuven, Belgium; fabien@ster.kuleuven.be

⁶ Observatoire de Genève, Ch. des Maillettes 51, CH-1290 Sauverny, Switzerland; patrick.eggenberger@obs.unige.ch

⁷ Laboratoire d'astrophysique, EPFL Observatoire CH-1290 Versoix; danuta.sosnowska@epfl.ch

⁸ McDonald Observatory, University of Texas at Austin, Austin, TX 78712, USA; robw@astro.as.utexas.edu, mike@astro.as.utexas.edu

⁹ High Altitude Observatory, National Centre for Atmospheric Research, Boulder, CO 80307-3000 USA; travis@ucar.edu

¹⁰ Leiden Observatory, Leiden University, 2300 RA Leiden, The Netherlands

¹¹ Royal Observatory of Belgium, 1180 Brussels, Belgium;

saskia@oma.be

¹² ZAH-Landessternwarte, 69117 Heidelberg, Germany; sreffert@lsw.uni-heidelberg.de

¹³ Carnegie Institution of Washington, Department of Terrestrial Magnetism, 5241 Broad Branch Road NW, Washington, DC 20015-1305; paul@dtm.ciw.edu

¹⁴ Anglo-Australian Observatory, P.O. Box 296, Epping, NSW 1710, Australia; otoole@aaoepp.aao.gov.au

¹⁵ Okayama Astrophysical Observatory, National Astronomical Observatory of Japan, National Institutes of Natural Sciences, 3037-5 Honjyo, Kamogata, Asakuchi, Okayama 719-0232, Japan; kambe@oao.nao.ac.jp, izumiura@oao.nao.ac.jp

¹⁶ National Astronomical Observatory of Japan, National Institutes of Natural Sciences, 2-21-1 Osawa, Mitaka, Tokyo 181-8588, Japan; ando@optik.mtk.nao.ac.jp

¹⁷ Global Edge Institute, Tokyo Institute of Technology 2-12-1-S6-6, Ookayama, Meguro-ku, Tokyo 152-8550, Japan; sato.b.aa@m.titech.ac.jp

¹⁸ Thüringer Landessternwarte Tautenburg, Sternwarte 5, 07778 Tautenburg, Germany; michael@tls-tautenburg.de, artie@tls-tautenburg.de

¹⁹ Institut d'Astrophysique de Paris, UMR7095, Université Pierre & Marie Curie, 98^{bis} Bd Arago, 75014 Paris, France; bouchy@iap.fr

²⁰ Observatoire de Paris, LESIA, UMR 8109, F-92195 Meudon, France; benoit.mosser@obspm.fr, caroline.barban@obspm.fr,

1. INTRODUCTION

Measuring solar-like oscillations in main-sequence and subgiant stars requires high-precision observations – either with spectroscopy or photometry – combined with coverage that is as continuous as possible. Most of the results have come from high-precision Doppler measurements using ground-based spectrographs, while measurements from spacecraft have also been reported (see Bedding & Kjeldsen 2007 and Aerts et al. 2008 for recent summaries).

Procyon has long been a favourite target for oscillation searches. At least eight separate velocity studies have reported an excess in the power spectrum, beginning with that by Brown et al. (1991), which was the first report of a solar-like power excess in another star. For the most recent examples, see Martić et al. (2004), Eggenberger et al. (2004), Bouchy et al. (2004) and Leccia et al. (2007). These studies agreed on the location of the excess power (around 0.5–1.5 mHz) but they disagreed on the individual oscillation frequencies. However, a consensus has emerged that the large separation (the frequency separation between consecutive overtone modes of a given angular degree) is about $55 \mu\text{Hz}$. Evidence for this value was first given by Mosser et al. (1998) and the first clear detection was made by Martić et al. (1999).

Controversy was generated when photometric observations obtained with the MOST satellite failed to reveal evidence for oscillations (Matthews et al. 2004; Guenther et al. 2007; Baudin et al. 2008). However, Bedding et al. (2005) argued that the MOST non-detection was consistent with the ground-based data. Meanwhile, Régulo & Roca Cortés (2005) suggested that the signature of oscillations is indeed present in the MOST data at a low level (see also Marchenko 2008). Using space-based photometry with the WIRE satellite, Bruntt et al. (2005) extracted parameters for the stellar granulation and found evidence for an excess due to oscillations.

All published velocity observations of Procyon have been made from a single site, with the exception of two-site observations by Martić et al. (2004). Here we

describe a multi-site campaign on Procyon carried out in 2007 January, which was the most extensive velocity campaign so far organized on any solar-type oscillator. The only other comparable effort to measure oscillations in this type of star was the multi-site photometric campaign of the open cluster M67 (Gilliland et al. 1993).

2. VELOCITY OBSERVATIONS

We observed Procyon from 2006 December 28 until 2007 January 23, using a total of eleven telescopes at eight observatories. These are listed in Table 1, ordered westward by longitude. Note that the FIES spectrograph on the Nordic Optical Telescope was still being commissioned during the observations and the velocity precision is therefore somewhat lower than for the other telescopes.

The team members from each telescope were responsible for producing a velocity time series from the observations, together with estimates of uncertainties. In six of the spectrographs, the stellar light was passed through an iodine absorption cell to provide a stable wavelength reference. In four others, wavelength calibration was achieved by recording the spectrum from a thorium-argon emission lamp alongside the stellar spectrum, while with EMILIE, exposures of the stellar spectrum were alternated with those of a white-light source passing through an iodine cell. Details of the methods used with each spectrograph are given in the references listed in Table 1 and details of the observations are given in Table 2.

The velocity time series of Procyon is shown in Fig. 1a, using a different color for each telescope. Differences between telescopes in the absolute zero point of velocity are not significant, and so all the curves have been shifted into alignment by subtracting a constant offset. This was done by setting the velocities from each telescope to have zero mean, excepting Lick and SARG, for which better alignment was achieved by setting the means to -6 m s^{-1} and -5 m s^{-1} , respectively. Note that EMILIE is not shown in Fig. 1a because those data were referenced to a different value on each night and so the night-to-night variations are not measurable (this does not affect their usefulness for oscillations studies, however). FIES is also not shown in Fig. 1a because it has much greater scatter than the rest.

In Fig. 1a we see variations in the radial velocity of Procyon on timescales of days. The good agreement between the different telescopes indicates that these slow variations have a stellar origin, although the imperfect match in overlapping sections shows that there is also a contribution from instrumental drifts. Figure 1b shows a close-up of the central part of the campaign, during which the coverage was above 90%. The solid curve shows the velocities after smoothing, to better reveal the slow variations, which are discussed in §4.1 below.

While interesting in their own right, the slow variations in the velocity series significantly affect our ability to detect oscillations, due to spectral leakage of power from the low-frequency part of the spectrum to the oscillation region at higher frequencies. Before merging the data from the individual telescopes, we therefore removed the low-frequency variations from the velocity series. This was done for each telescope by removing all the power below $280 \mu\text{Hz}$, a value that was chosen so as to effectively remove the slow variations without affecting the

eric.michel@obspm.fr

²¹ Institut d'Astrophysique Spatiale, Université Paris XI-CNRS, Bâtiment 121, 91405 Orsay cedex, France; Thierry.Appourchaux@ias.u-psud.fr

²² Laboratoire Cassiopée, UMR CNRS 6202, Observatoire de la Côte d'Azur, BP 4229, 06304 Nice cedex 4, France; Gabrielle.Berthomieu@obs-nice.fr, Janine.Provost@obs-nice.fr

²³ DAPNIA/DSM/Service d'Astrophysique, CEA/Saclay, 91191 Gif-sur-Yvette Cedex, France; rafael.garcia@cea.fr, sylvaine.turkchieze@cea.fr

²⁴ Service d'Aéronomie du CNRS, BP 3, 91371 Verrières le Buisson, France; milena.martić@aerov.jussieu.fr, jean-claude.lebrun@aerov.jussieu.fr, jean-loup.beraux@aerov.jussieu.fr

²⁵ Observatoire de Haute Provence, 04870 St Michel l'Observatoire, France; jerome.schmitt@oamp.fr

²⁶ INAF - Osservatorio Astrofisico di Catania, via S. Sofia 78, 95123 Catania, Italy; abo@oact.inaf.it, rco@ct.astro.it

²⁷ INAF - Astronomical Observatory of Padua, Vicolo Osservatorio 5, 35122 Padova, Italy; serena.benatti@oapd.inaf.it, riccardo.claudi@oapd.inaf.it

²⁸ INAF - Astronomical Observatory of Capodimonte, Salita Moiarriello 16, 80131 Napoli, Italy; leccia@na.astro.it

²⁹ School of Physics & Astronomy, University of St. Andrews, North Haugh, St. Andrews KY16 9SS, Scotland; Eric.Stempels@st-andrews.ac.uk

oscillation signal. This filtering was done by subtracting a smoothed version of the time series that contained all the power below that cut-off frequency.

In Fig. 1c we show a close-up of a segment during which three spectrographs were observing simultaneously. The stellar oscillations are clearly visible, with typical periods of about 15 minutes, and there is good agreement between the different telescopes. Note that these data have been filtered to remove the slow variations.

3. OPTIMIZING THE WEIGHTS

The procedures for extracting velocities for each telescope also produced estimates of the uncertainties, σ_i . In our analysis, we used these uncertainties to calculate noise-optimized weights in the usual way, namely $w_i = 1/\sigma_i^2$. If weights are not used when calculating the power spectrum, a few bad data points can dominate and increase the noise floor significantly.

We now describe the process we used to adjust these weights, which aims to minimize the noise level in the final power spectrum. The procedure involves identifying and revising those uncertainties that were too optimistic, and at the same time rescaling the uncertainties to be in agreement with the actual noise levels in the data. These methods have already been described in previous papers (Butler et al. 2004; Bedding et al. 2007; Leccia et al. 2007), but the present analysis differs slightly from those descriptions and we will therefore describe them in some detail. One difference is that the analysis had to be tailored to the individual time series because of the large range of Nyquist frequencies (see Table 2).

To illustrate the process, we show in Figs. 2 and 3 segments of data at different stages in the process for two telescopes (HARPS and EMILIE). The top panels (Figs. 2a and 3a) show the velocities for a single night, with the slow variations removed. The remaining panels show the uncertainties at different stages in the analysis.

It is important to stress that we are not adjusting the velocities, only the uncertainties. Of course, those adjustments still affect the power spectrum of the velocities (which is, after all, why we are making the adjustments) and so it is important to ensure that they do not distort the oscillation signal and that the final weights reflect as accurately as possible the actual noise properties of the series.

3.1. Scaling the uncertainties

We have scaled the uncertainties so that they agree with the noise level in the corresponding amplitude spectrum, σ_{amp} , as measured at high frequencies. This was done for each night and each telescope by multiplying the uncertainties, σ_i , by a constant so that they satisfied equation (3) of Butler et al. (2004):

$$\sigma_{\text{amp}}^2 \sum_{i=1}^N \sigma_i^{-2} = \pi. \quad (1)$$

This scaling was repeated after each step in the process described below. Figures 2b and 3b show the uncertainties after scaling, and before any further adjustments.

3.2. Filtering the uncertainties

It is clear that the uncertainties in some parts of the time series show variations that correlate with the oscillations of Procyon. The clearest example is HARPS, as shown by comparing the top two panels of Fig. 2, but the effect is also visible for other telescopes (e.g., Fig 3). To remove this structure in the uncertainties, we have bandpass-filtered each of the uncertainty time series to remove all power in the frequency range 280–2200 μHz . This removed fluctuations in the weights on the timescale of the stellar oscillations, while retaining information on longer timescales (such as poorer conditions at the beginnings and ends of nights) and on shorter timescales (such as individual bad data points). This process resulted in slightly lower noise levels in the final power spectra for some of the individual telescopes, reflecting the fact that the uncertainties, like any measurement, contain noise that is reduced by bandpass filtering. Figures 2c and 3c show the uncertainties after filtering.

We also noticed a few data points (~ 10) with unrealistically *low* uncertainties. These points would be given too high a weight in the analysis and the uncertainties were therefore reset to the mean uncertainty for that telescope night.

3.3. Down-weighting bad data points

Down-weighting of bad data points was done following the method described by Butler et al. (2004), with one difference that is discussed below. The first step was to make a high-pass-filtered version of the velocity time series in which both the slow variations and the stellar oscillations were removed. This gave us a series of residual velocities, r_i , in which we could identify data points that needed to be down-weighted, without being affected by spectral leakage from the oscillations. The frequency limit of this high-pass filter varied from telescope to telescope, depending on the Nyquist frequency of the data.

We compared the velocity residuals, r_i , with the corresponding uncertainty estimates, σ_i . Bad data points are those for which the ratio $|r_i/\sigma_i|$ is large, i.e., where the residual velocity deviates from zero by more than expected from the uncertainty estimate. Butler et al. (2004), who analyzed data similar to ours, found that the fraction of good data points was essentially unity up to $|r_i/\sigma_i| = 2$ and then dropped off quickly for larger values of $|r_i/\sigma_i|$ – see Figure 3 of Butler et al. (2004). They therefore introduced the factor f , which is the fraction of good data points as a function of $|r_i/\sigma_i|$ and which they obtained as the ratio between the distribution of data points in a cumulative histogram of $|r_i/\sigma_i|$ and a best-fit Gaussian distribution.

We used a slightly different approach. With the knowledge that points with large values of $|r_i/\sigma_i|$ are bad, we introduced an analytical function

$$f(x_i) = \frac{1}{1 + \left(\frac{x_i}{x_0}\right)^{10}}, \quad x_i = |r_i/\sigma_i|, \quad (2)$$

which has shape very similar to the fraction f as a function of $|r_i/\sigma_i|$ in Butler et al. (2004). The adjustable parameter x_0 controls the amount of down-weighting; it sets the value of $|r_i/\sigma_i|$ for which the weights are multiplied by 0.5, and so it determines how bad a data point should be before it is down-weighted. The optimum

choice for x_0 was found through iteration, as described below. Once this was done, we used $f(x_i)$ to adjust the weights by dividing σ_i by $\sqrt{f(x_i)}$, as in Butler et al. (2004).

The noise level used for optimizing x_0 was measured in a frequency band near 2 mHz in a weighted amplitude spectrum, between the oscillations and the high-frequency part of the spectrum used for determining the $|r_i/\sigma_i|$ values. The exact position of the band was chosen for each spectrograph separately, because of the differences in Nyquist frequencies. For each trial value of x_0 , the noise level was determined from a time series in which all power had been removed at both the low- and high-frequency side of the frequency band, i.e., from a bandpass-filtered time series containing information in the specific frequency band only. This was done because applying the weights changes the spectral window function and thus the amount of spectral leakage into the frequency band where we determine the noise: if we did not filter out the oscillations and the high-frequency part of the spectrum, we would optimize for a combination of low noise *and* minimum amount of spectral leakage (from both the low- and high frequency side of the passband). In other words, the spectral window function would influence our choice of x_0 , which is not optimal for obtaining the lowest possible noise level.

The procedure described above was repeated for a range of x_0 values and we chose the one that resulted in the lowest noise in the power spectrum. Depending on the telescope, and hence the noise properties of the time series, the optimal values of x_0 ranged from 1.7 to 4.3. Figures 2d and 3d show the final uncertainties for HARPS and EMILIE.

This completes our description of the process used to adjust the uncertainties. The results from calculating weighted power spectra using these uncertainties are presented in §4.2. First, however, we discuss the slow variations in the velocity of Procyon that are present in our data.

4. RESULTS

4.1. Slow variations in stellar velocity

The slow variations in the radial velocity of Procyon seen in Fig. 1 are remarkably similar to those seen in the Sun. This can be seen from Fig. 4, which shows a typical time series of solar velocity measurements made with the GOLF instrument on the SOHO spacecraft (Ulrich et al. 2000; García et al. 2005). Longer series of GOLF data show variations with a period of about 13 d arising from active regions crossing the solar disk (Fig. 11 in García et al. 2005; see also Tingley et al. 2008). This 13-day periodicity in solar velocities was first observed by Claverie et al. (1982), who attributed it to rapid rotation of the core, but it was subsequently shown to be due to surface rotation of active regions (Durrant & Schröter 1983; Andersen & Maltby 1983; Edmunds & Gough 1983). Similarly, we attribute the slow variations in the radial velocity of Procyon to the appearance and disappearance of active regions and their rotation across the stellar disk. This explanation was also invoked by Mosser et al. (2005) to explain much larger velocity variations measured with HARPS for the COROT target HR 2530 (= HD 49933; spectral type

F5 V).

The slow variations in Procyon appear to have a period of $P_{\text{slow}} = 10.3 \pm 0.5$ d, as measured from the highest peak in the power spectrum. This agrees with an apparent periodicity of about 10 d in two-site observations of Procyon obtained over 20 nights by Kambe et al. (2008, see their Fig. 12). Identifying this as the stellar rotation period and using a radius of $2.05 R_{\odot}$ (Kervella et al. 2004) implies a surface rotational speed at the equator of $v = 10 \pm 0.5 \text{ km s}^{-1}$. The measured value of P_{slow} period might also correspond to half the rotation period (Clarke 2003), in which case the rotational speed would be half the value given above. Combining with the spectroscopic value of $v \sin i = 3.16 \pm 0.50 \text{ km s}^{-1}$ (Allende Prieto et al. 2002) gives an inclination angle of $i = 18 \pm 3^\circ$ (if $P_{\text{rot}} = P_{\text{slow}}$) and $i = 39 \pm 7^\circ$ (if $P_{\text{rot}} = 2P_{\text{slow}}$). The inclination of the binary orbit is $31.1 \pm 0.6^\circ$ (Girard et al. 2000) and so, if we require that the rotation axis of Procyon is aligned with the orbital rotation axis, it may be that $P_{\text{rot}} = 2P_{\text{slow}}$.

4.2. Power spectra and stellar activity

The weighted power spectrum for each telescope and for the combined time series, based on the uncertainties discussed in §3, are shown in Fig. 5. The noise levels, as measured at high frequencies in the amplitude spectrum (σ_{amp}), are given in column 8 of Table 2. The final column of that table gives the mean noise level per minute of observing time, with a spread that reflects a combination of factors, including telescope aperture, observing duty cycle, spectrograph design, as well as atmospheric conditions such as seeing.

The power spectrum of the combined time series is shown again in Fig. 6, both with and without the use of weights. As is well-established, using weights reduces the noise level significantly, at the cost of increasing the sidelobes in the spectral window (because the best data segments are given more weight – see insets). When weights are used, the noise level above 3 mHz is 1.9 cm s^{-1} in amplitude, but this does include some degree of spectral leakage from the oscillations. If we high-pass filter the spectrum up to 3 mHz, the noise level drops to 1.5 cm s^{-1} in amplitude. Note that without the use of weights, the noise level is higher by more than a factor of two.

Looking again at Fig. 6, we see that the use of weights appears to have increased the amplitude of the oscillations. In fact, this indicates the finite lifetime of the oscillation modes: in Fig. 6b the HARPS data are given the highest weight, and so the effective duration of the observations is decreased (and the sidelobes in the spectral window become much stronger). Our estimate of the mode lifetime is given in §4.3.

It is also useful to convert to power density, which is independent of the observing window and therefore allows us to compare noise levels. This is done by multiplying the power spectrum by the effective length of the observing run, which we calculate as the reciprocal of the area integrated under the spectral window (in power). The values for the different telescopes are given in column 3 of Table 2. In Fig. 7 we show the power density spectrum on a logarithmic scale for the HARPS data, which has the lowest noise per minute of observing time. We see three components: (i) the oscillations (about 300–1100 μHz);

(ii) white noise at high frequencies; and (iii) a sloping background of power at low frequencies (stellar granulation and activity, and presumably also some instrumental drift). Figure 8 compares the power density spectra for the different telescopes. They show a similar oscillation signal and similar background from stellar noise at lower frequencies (below about $250 \mu\text{Hz}$), with different levels of white noise at higher frequencies (above about $2000 \mu\text{Hz}$), reflecting the different levels of photon noise.

In Fig. 7, the lower two dashed lines indicate the background level in the Sun, as measured from the GOLF data during solar minimum and maximum, respectively. The upper dashed line is the solar maximum line shifted to match the power density of Procyon, which required multiplying by a factor of 40. We can use this scaling factor to estimate the fraction of Procyon's surface that is covered by active regions, relative to the Sun, as follows. The low-frequency part of the velocity power-density spectrum from the Sun falls off as frequency squared (Harvey 1985; Pallé et al. 1999), and we see the same behaviour for Procyon. Hence, in both cases we have

$$PD(\nu) \propto \nu^{-2}. \quad (3)$$

Let T be the typical time for an active region to be visible on the surface (which may depend on both rotation and the typical lifetime of active regions). The amplitude of the velocity signal at frequency $\nu_0 = 1/T$ will be proportional to the fractional area covered by active regions, da/a , and to the projected rotational velocity, $v \sin i$. The power density at ν_0 is therefore:

$$PD(\nu_0) = (da/a)^2 (v \sin i)^2. \quad (4)$$

Combining these gives

$$PD(\nu) = \left(\frac{da}{a}\right)^2 \left(\frac{v \sin i}{T}\right)^2 \nu^{-2}. \quad (5)$$

We will assume that T is proportional to the rotation period, which we take to be 10.3 d (or twice that value) for Procyon and 25.4 d for the Sun. The measured values for $v \sin i$ are 3.2 km s^{-1} for Procyon (Allende Prieto et al. 2002) and 2.0 km s^{-1} for the Sun. Combining these values with our measurement of the power densities indicates that the area covered by active regions on Procyon is about 1.6 times the solar maximum value (or twice that value). No detection of a magnetic field in Procyon has been reported, and published upper limits imply that the average field cannot be more than a few times solar (see Table 3 in Kim et al. 2007), which appears to be consistent with our results.

4.3. Oscillation amplitude and mode lifetime

To measure the amplitude of oscillations in Procyon, we have used the method described by Kjeldsen et al. (2008). In brief, this involves the following steps: (i) heavily smoothing the power spectrum (by convolving with a Gaussian having a full width at half maximum of $4\Delta\nu$, where $\Delta\nu$ is the large frequency separation), to produce a single hump of excess power that is insensitive to the fact that the oscillation spectrum has discrete peaks; (ii) converting to power density (see §4.2); (iii) fitting and subtracting the background noise; and (iv) multiplying by $\Delta\nu/4.09$ and taking the square root, in order

to convert to amplitude per radial oscillation mode. Note that 4.09 is the effective number of modes per order for full-disk velocities observations, normalized to the amplitudes of radial ($l = 0$) modes – see Kjeldsen et al. (2008) for details.

We applied this method to each of the telescopes separately, and the result is shown in Fig. 9. There are significant differences between the different curves, which we attribute to intrinsic variations in the star arising from the stochastic nature of the excitation and damping. To investigate this further, we also applied the method to the combined time series, after first subdividing it into ten 2-day subsets. Figure 10 shows these amplitude curves and also their average.

The amplitude curve of Procyon has a broad plateau, rather than the single peak that has been seen for other stars. Figure 11 shows the smoothed amplitude curve for Procyon compared to the Sun and other stars. It is an updated version of Fig. 8 of Kjeldsen et al. (2008), where the following stars have been added: μ Ara (Bouchy et al. 2005), HD 49933 (Mosser et al. 2005), μ Her (Bonanno et al. 2008), γ Pav (Mosser et al. 2008b), τ Cet (Teixeira et al. 2008).

The plateau for Procyon is centred at $900 \mu\text{Hz}$ and is about $500 \mu\text{Hz}$ wide, with a mean amplitude across that range of $38.1 \pm 1.3 \text{ cm s}^{-1}$. This is our estimate for the amplitude of the radial ($l = 0$) modes in Procyon. Comparing with the corresponding measurement for the Sun ($18.7 \pm 0.7 \text{ cm s}^{-1}$; Kjeldsen et al. 2008) implies that the velocity oscillations in Procyon are 2.04 ± 0.10 times solar. In both Procyon and the Sun, the modes with $l = 1$ are higher by a factor of 1.35 (see Table 1 of Kjeldsen et al. 2008).

The corresponding intensity amplitude, after accounting for the higher effective temperature of Procyon (see Eq. 5 in Kjeldsen & Bedding 1995), is 1.60 times solar. This implies an amplitude at 500 nm of 6.8 ppm for $l = 0$ and 8.5 ppm for $l = 1$ (see Table 1 of Kjeldsen et al. 2008). These amplitudes are completely consistent with the detection of oscillations in Procyon by WIRE (Bruntt et al. 2005) and with the upper limit set by MOST (Matthews et al. 2004; Bedding et al. 2005).

The standard deviation of the ten segments in Fig. 10 is $\sigma_A/A = 10.4\% \pm 2.3\%$, which reflects the finite lifetime of the modes. We can use equation (3) from Kjeldsen et al. (2008) to estimate the mode lifetime, but we must account for the much greater width of the oscillation envelope in Procyon. Note that this equation was established empirically and we have confirmed it analytically using the work of Toutain & Appourchaux (1994). We estimate the mode lifetime to be $\tau = 1.5^{+1.9}_{-0.8} \text{ d}$. This equals, within rather large uncertainties, the solar value of 2.9 d (e.g., Chaplin et al. 1997).

5. CONCLUSIONS

We have presented multi-site velocity observations of Procyon that we obtained with eleven telescopes over more than three weeks. Combining data that spans a range of precisions and sampling rates presents a significant challenge. When calculating the power spectrum, it is important to use weights that are based on the measurement uncertainties, otherwise the result is dominated by the noisiest data. We have described in detail our methods for adjusting the weights in order to minimize

the noise level in the final power spectrum.

Our velocity measurements show the clear signature of oscillations. The power spectrum shows an excess in a plateau that is centred at 0.9 mHz and is broader than has been seen for other solar-type stars. The mean amplitude of the radial modes is $38.1 \pm 1.3 \text{ cm s}^{-1}$ (2.04 ± 0.10 times solar), which is consistent with previous detections from the ground and by the WIRE spacecraft, and also with the upper limit set by the MOST spacecraft. The variation of the amplitude during the observing campaign allowed us to estimate the mode lifetime to be $1.5^{+1.9}_{-0.8} \text{ d}$.

We also found a slow variation in the radial velocity of Procyon, with good agreement between different telescopes. These variations are remarkably similar to those seen in the Sun, and we interpret them as being due to rotational modulation from active regions on the stellar surface. The variations appear to have a period of about 10 days, which presumably equals the stellar rotation period or, perhaps, half of it. The amount of power in these slow variations indicates that the fractional area of Pro-

cyon covered by active regions is slightly higher than for the Sun.

The excellent coverage of the observations and the high signal-to-noise should allow us to produce a good set of oscillation frequencies for Procyon. This analysis will be presented in subsequent papers.

This work was supported financially by the Danish Natural Science Research Council, the Australian Research Council, the Swiss National Science Foundation, NSF grant AST-9988087 (RPB) and by SUN Microsystems. We thank Hugh Jones, Chris Tinney and the other members of the Anglo-Australian Planet Search for agreeing to a time swap that allowed our AAT observations to be scheduled. MM is grateful to Prof. N. Kameswara Rao, G. Pandey and S. Sriram for their participation in campaign with VBT Echelle Spectrometer, which was used for the first time for Doppler spectroscopy observations.

REFERENCES

- Aerts, C., Christensen-Dalsgaard, J., Cunha, M., & Kurtz, D. W., 2008, *Sol. Phys.* in press (arXiv:0803.3527).
- Allende Prieto, C., Asplund, M., López, R. J. G., & Lambert, D. L., 2002, *ApJ*, 567, 544.
- Andersen, B. N., & Maltby, P., 1983, *Nat*, 302, 808.
- Baudin, F., Appourchaux, T., Boumier, P., Kuschnig, R., Leibacher, J. W., & Matthews, J. M., 2008, *A&A*, 478, 461.
- Bedding, T. R., & Kjeldsen, H., 2007, In Stancliffe, R. J., Houdek, G., Martin, R. G., & Tout, C. A., editors, *Unsolved Problems in Stellar Physics: A Conference in Honour of Douglas Gough*, volume 948, page 117. American Institute of Physics.
- Bedding, T. R., Kjeldsen, H., Arentoft, T., et al., 2007, *ApJ*, 663, 1315.
- Bedding, T. R., Kjeldsen, H., Bouchy, F., et al., 2005, *A&A*, 432, L43.
- Bonanno, A., Benatti, S., Claudi, R., Desidera, S., Gratton, R., Leccia, S., & Paternò, L., 2008, *ApJ*, 676, 1248.
- Bouchy, F., Bazot, M., Santos, N. C., Vauclair, S., & Sosnowska, D., 2005, *A&A*, 440, 609.
- Bouchy, F., & Carrier, F., 2002, *A&A*, 390, 205.
- Bouchy, F., Maeder, A., Mayor, M., Mégevand, D., Pepe, F., & Sosnowska, D., 2004, *Nat*, 432, 7015.
- Bouchy, F., Schmitt, J., Bertaux, J.-L., & Connes, P., 2002, In Aerts, C., Bedding, T. R., & Christensen-Dalsgaard, J., editors, *IAU Colloquium 185: Radial and Nonradial Pulsations as Probes of Stellar Physics*, volume 259, page 472. ASP Conf. Ser.
- Brown, T. M., Gilliland, R. L., Noyes, R. W., & Ramsey, L. W., 1991, *ApJ*, 368, 599.
- Brunth, H., Kjeldsen, H., Buzasi, D. L., & Bedding, T. R., 2005, *ApJ*, 633, 440.
- Butler, R. P., Bedding, T. R., Kjeldsen, H., et al., 2004, *ApJ*, 600, L75.
- Butler, R. P., Marcy, G. W., Williams, E., McCarthy, C., Dosanji, P., & Vogt, S. S., 1996, *PASP*, 108, 500.
- Chaplin, W. J., Elsworth, Y., Isaak, G. R., McLeod, C. P., Miller, B. A., & New, R., 1997, *MNRAS*, 288, 623.
- Clarke, D., 2003, *A&A*, 407, 1029.
- Claudi, R. U., Bonanno, A., Leccia, S., Ventura, R., Desidera, S., Gratton, R., Cosentino, R., Paterno, L., & Endl, M., 2005, *A&A*, 429, L17.
- Claverie, A., Isaak, G. R., McLeod, C. P., van der Raay, H. B., Palle, P. L., & Roca Cortes, T., 1982, *Nat*, 299, 704.
- Durrant, C. J., & Schröter, E. H., 1983, *Nat*, 301, 589.
- Edmunds, M. G., & Gough, D. O., 1983, *Nat*, 302, 810.
- Eggenberger, P., Carrier, F., Bouchy, F., & Blecha, A., 2004, *A&A*, 422, 247.
- Endl, M., Cochran, W. D., Hatzes, A. P., & Wittenmyer, R. A., 2005, In *Revista Mexicana de Astronomía y Astrofísica Conference Series*, volume 23, page 64.
- Frandsen, S., & Lindberg, B., 2000, In Teixeira, T., & Bedding, T. R., editors, *The Third MONS Workshop: Science Preparation and Target Selection*, page 163. Aarhus: Aarhus Universitet.
- García, R. A., Turck-Chièze, S., Boumier, P., Robillot, J. M., Bertello, L., et al., 2005, *A&A*, 442, 385.
- Gilliland, R. L., Brown, T. M., Kjeldsen, H., McCarthy, J. K., Peri, M. L., et al., 1993, *AJ*, 106, 2441.
- Girard, T. M., Wu, H., Lee, J. T., Dyson, S. E., van Altena, W. F., et al., 2000, *AJ*, 119, 2428.
- Guenther, D. B., Kallinger, T., Reegen, P., Weiss, W. W., Matthews, J. M., Kuschnig, R., Moffat, A. F. J., Rucinski, S. M., Sasselov, D., & Walker, G. A. H., 2007, *Commun. Asteroseismology*, 151, 5.
- Harvey, J., 1985, In Rolfe, E., & Battrick, B., editors, *Future Missions in Solar, Heliospheric & Space Plasma Physics*, ESA SP-235, page 199.
- Hatzes, A. P., Guenther, E., Kürster, M., & McArthur, B., 2003, In Fridlund, M., Henning, T., & Lacoste, H., editors, *Earth's DARWIN/TPF and the Search for Extrasolar Terrestrial Planets*, volume 539, page 441.
- Kambe, E., Ando, H., Sato, B., et al., 2008, *PASJ*, 60, 45.
- Kervella, P., Thévenin, F., Morel, P., Berthomieu, G., Bordé, P., & Provost, J., 2004, *A&A*, 413, 251.
- Kim, K.-M., Han, I., Valyavin, G. G., Plachinda, S., Jang, J. G., et al., 2007, *PASP*, 119, 1052.
- Kjeldsen, H., & Bedding, T. R., 1995, *A&A*, 293, 87.
- Kjeldsen, H., Bedding, T. R., Arentoft, T., et al., 2008, *ApJ* in press, arXiv:0804.1182.
- Leccia, S., Kjeldsen, H., Bonanno, A., Claudi, R. U., Ventura, R., & Paternò, L., 2007, *A&A*, 464, 1059.
- Marchenko, S. V., 2008, *A&A*, 479, 845.
- Martić, M., Lebrun, J.-C., Appourchaux, T., & Korzennik, S. G., 2004, *A&A*, 418, 295.
- Martić, M., Schmitt, J., Lebrun, J.-C., Barban, C., Connes, P., Bouchy, F., Michel, E., Baglin, A., Appourchaux, T., & Bertaux, J.-L., 1999, *A&A*, 351, 993.
- Matthews, J. M., Kuschnig, R., Guenther, D. B., et al., 2004, *Nat*, 430, 51. Erratum: 430, 921.
- Mosser, B., Bouchy, F., Catala, C., et al., 2005, *A&A*, 431, L13.
- Mosser, B., Bouchy, F., Martić, M., Appourchaux, T., Barban, C., et al., 2008a, *A&A*, 478, 197.
- Mosser, B., Deheuvels, S., Michel, E., Thevenin, F., Dupret, M. A., Samadi, R., Barban, C., & Goupil, M. J., 2008b, *A&A* in press (2008arXiv0804.3119).

- Mosser, B., Maillard, J. P., Mékarnia, D., & Gay, J., 1998, A&A, 340, 457.
- Pallé, P. L., Roca Cortés, T., Jiménez, A., Golf, & VIRGO Teams, 1999, In Giménez, A., Guinan, E. F., & Montesinos, B., editors, *Proc. Workshop on Stellar Structure theory and Tests of Convective Energy Transport*, volume 173, page 297. ASP Conf. Ser.
- Régulo, C., & Roca Cortés, T., 2005, A&A, 444, L5.
- Rupprecht, G., Pepe, F., Mayor, M., et al., 2004, In Moorwood, A. F. M., & Masanori, I., editors, *Ground-based Instrumentation for Astronomy*, volume 5492 of *Proc. SPIE*, page 148.
- Teixeira, T., Kjeldsen, H., Bedding, T. R., et al., 2008, A&A. to be submitted.
- Tingley, B., Grundahl, F., & Kjeldsen, K., 2008, MNRAS. to be submitted.
- Toutain, T., & Appourchaux, T., 1994, A&A, 289, 649.
- Ulrich, R. K., García, R. A., Robillot, J.-M., Turck-Chièze, S., Bertello, L., Charra, J., Dzitko, H., Gabriel, A. H., & Roca Cortés, T., 2000, A&A, 364, 799.

TABLE 1
PARTICIPATING TELESCOPES

Identifier	Telescope/Spectrograph	Observatory	Technique	Ref.
HARPS	3.6 m/HARPS	ESO, La Silla, Chile ^a	ThAr	1
CORALIE	1.2 m Euler Telescope/CORALIE	ESO, La Silla, Chile	ThAr	2
McDonald	2.7 m Harlan J. Smith Tel./coudé échelle	McDonald Obs., Texas USA	iodine	3
Lick	0.6 m CAT/Hamilton échelle	Lick Obs., California USA	iodine	4
UCLES	3.9 m AAT/UCLES	Siding Spring Obs., Australia	iodine	4
Okayama	1.88 m/HIDES	Okayama Obs., Japan	iodine	5
Tautenburg	2 m/coudé échelle	Karl Schwarzschild Obs., Germany	iodine	6
SOPHIE	1.93 m/SOPHIE	Obs. de Haute-Provence, France	ThAr	7
EMILIE	1.52 m/EMILIE+AAA	Obs. de Haute-Provence, France	white light with iodine	8
SARG	3.58 m TNG/SARG	ORM, La Palma, Spain	iodine	9
FIES	2.5 m NOT/FIES	ORM, La Palma, Spain	ThAr	10

1. Rupprecht et al. (2004); 2. Bouchy & Carrier (2002); 3. Endl et al. (2005); 4. Butler et al. (1996);
5. Kambe et al. (2008); 6. Hatzes et al. (2003); 7. Mosser et al. (2008a); 8. Bouchy et al. (2002) and paper in prep.;
9. Claudi et al. (2005); 10. Frandsen & Lindberg (2000)

^aBased on observations collected at the European Southern Observatory, La Silla, Chile (ESO Programme 078.D-0492 (A)).

TABLE 2
SUMMARY OF OBSERVATIONS

Identifier	Nights Allocated	Eff. Obs. time (h)	Spectra	Median t_{exp} (s)	Deadtime (s)	f_{Nyq} (mHz)	Noise Level (cm s ⁻¹)	Noise per Minute (m s ⁻¹)
HARPS	8	52.0	5698	5	31	13.8	2.0	0.64
CORALIE	6	27.0	936	40	85	4.0	9.8	2.2
McDonald	6	16.2	1719	17	15	15.6	14.4	2.5
Lick	14	95.4	1900	180	54	2.1	10.9	4.7
UCLES	12	41.4	2451	16	45	8.2	6.6	1.9
Okayama	20	83.4	1997	54	110	3.1	8.0	3.2
Tautenburg	21	14.6	494	60	65	4.0	22.8	3.8
SOPHIE	9	35.1	3924	23	28	9.7	4.7	1.2
EMILIE	4	25.7	1631	47	17	7.8	10.1	2.2
SARG	4	15.2	693	19	65	5.9	12.6	2.1
FIES	10 × $\frac{1}{2}$	12.6	1087	18	45	7.9	21.7	3.4

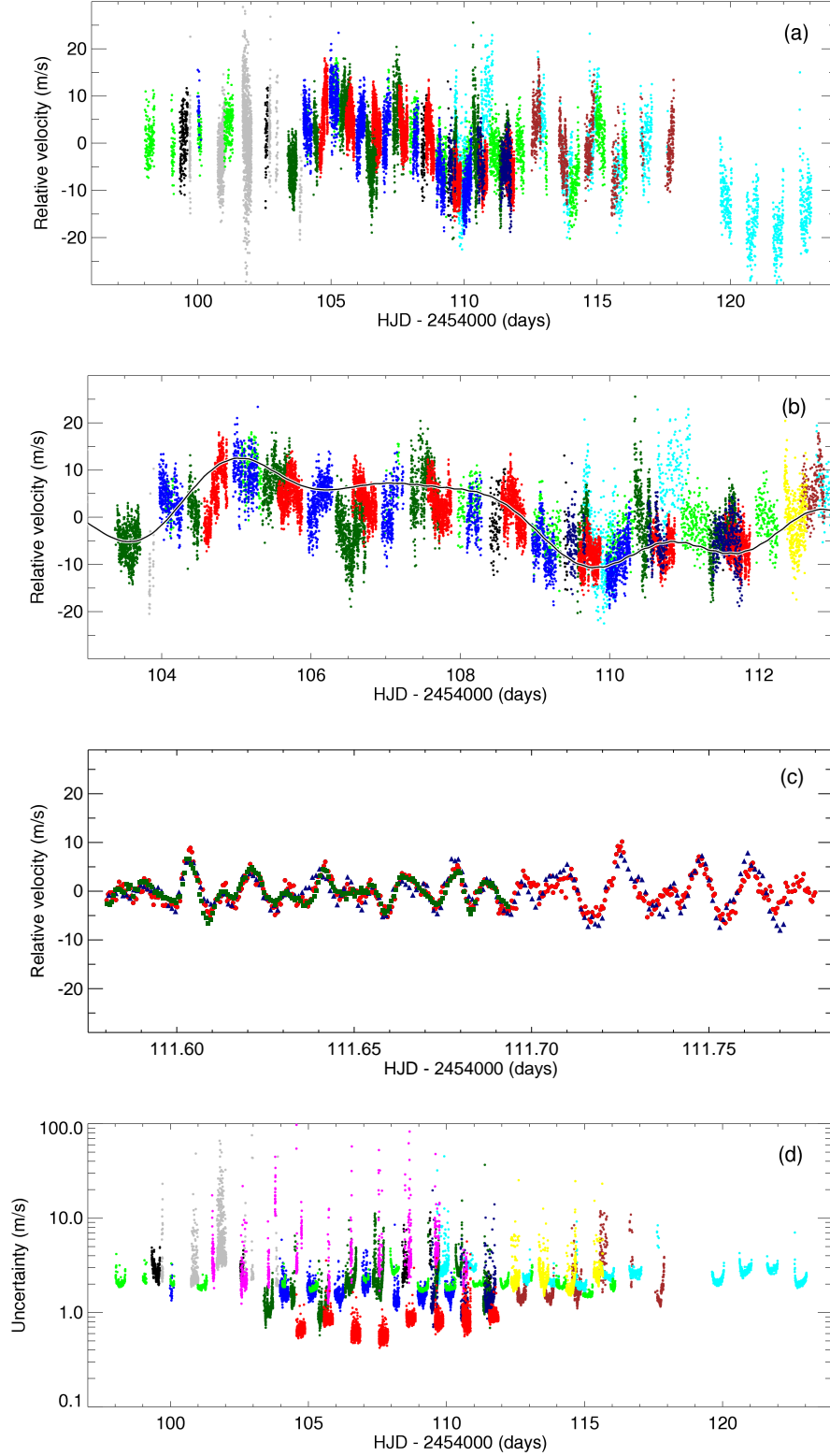


FIG. 1.— Velocity measurements of Procyon, color-coded as follows: HARPS = red; CORALIE = brown; McDonald = gray; Lick = cyan; UCLES = blue; Okayama = green; Tautenburg = black; SOPHIE = dark green; SARG = dark blue; FIES = magenta; EMILIE = yellow. (a) The full time series, before any removal of slow trends (EMILIE and FIES are not shown). (b) Close-up of the central ten days (FIES not shown). (c) Close-up of a five-hour segment during which three spectrographs observed simultaneously: HARPS (red circles), SOPHIE (dark green squares) and SARG (dark blue triangles). All three series have been high-pass filtered to remove slow trends and the SOPHIE and SARG data have been smoothed slightly (using a boxcar with a width of three data points). (d) The time series of the final noise-optimized uncertainties, showing all 11 telescopes.

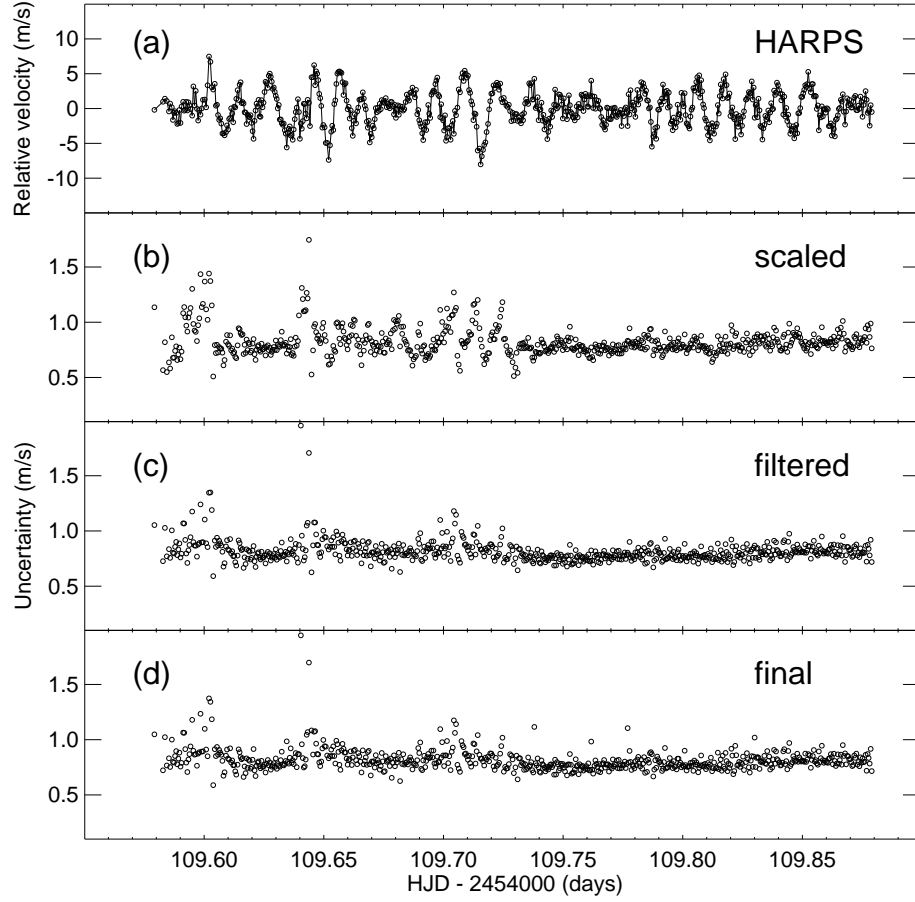


FIG. 2.— Steps in the adjustments of weights, illustrated using HARPS data from a single night. (a) The velocities, with the slow variations removed. (b) The uncertainties, after scaling to satisfy Eq. 1 but before any further adjustments. (c) The uncertainties after filtering to remove power on the timescale of the oscillations. (d) The final uncertainties, after adjusting to optimize the noise (see text).

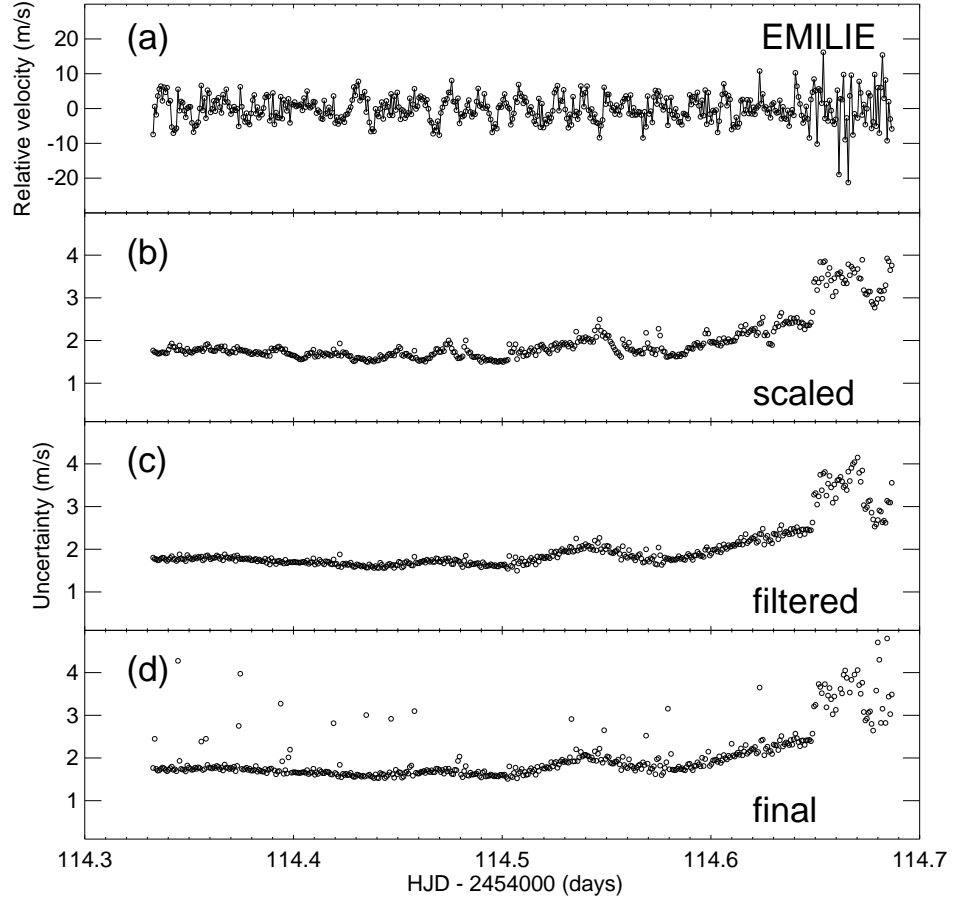


FIG. 3.— Same as Fig. 2, but for a single night from EMILIE.

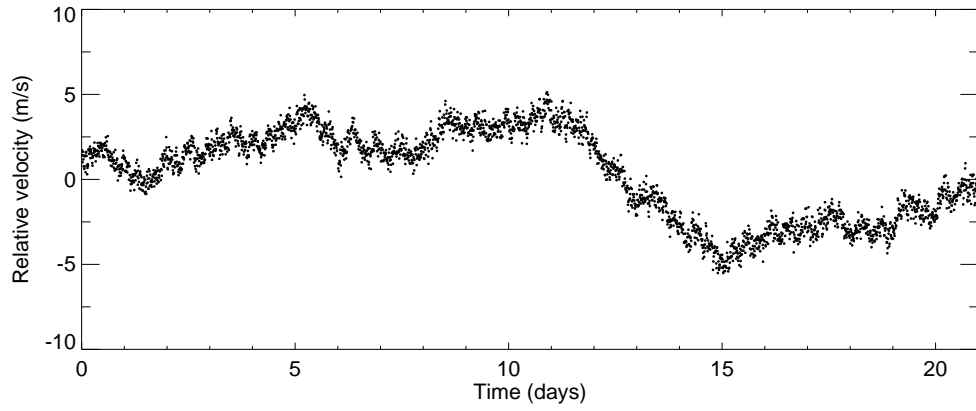


FIG. 4.— Time series of velocity measurements of the Sun obtained over 21 days with the GOLF instrument on the SOHO spacecraft.

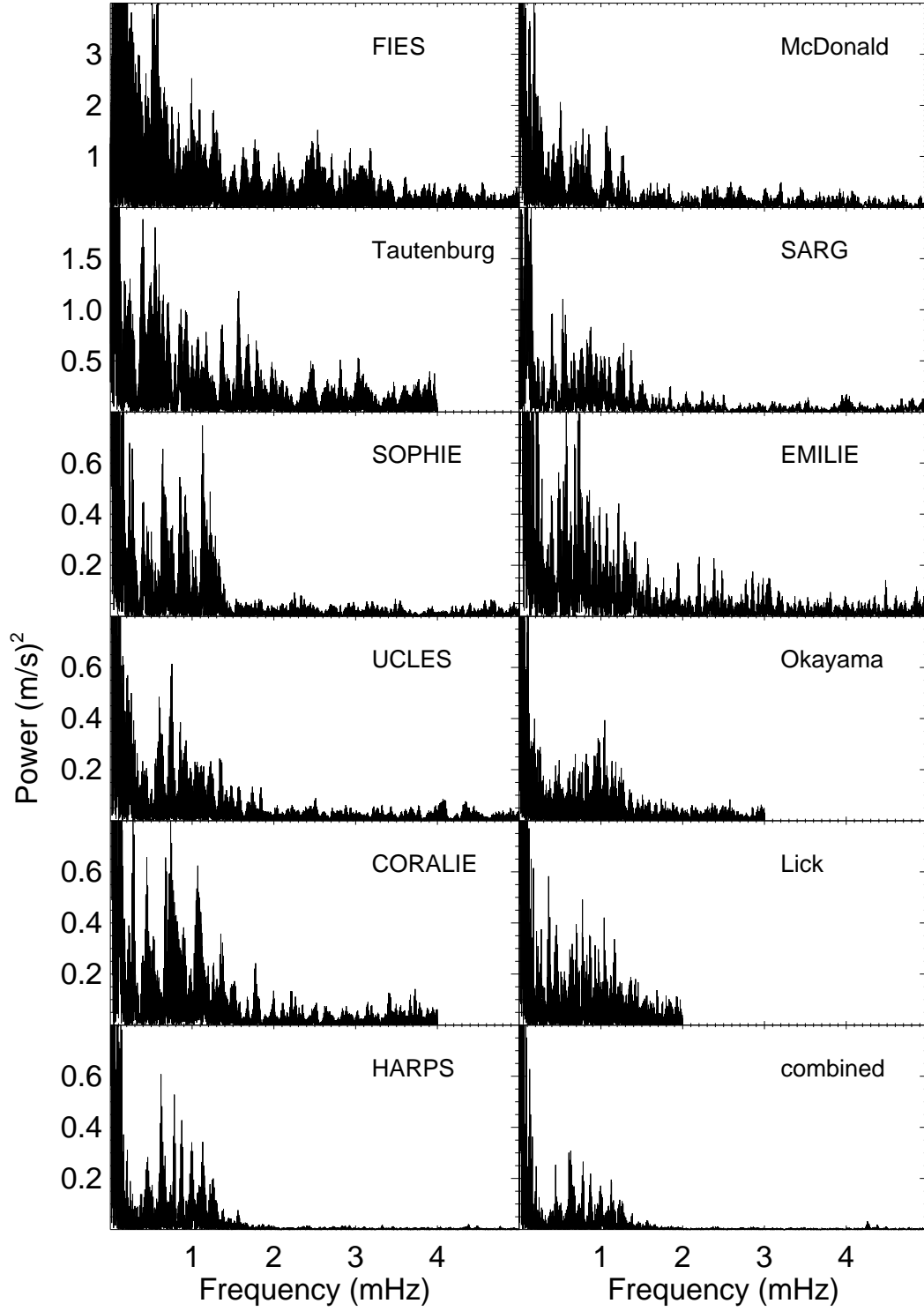


FIG. 5.— Power spectra for all 11 telescopes, together with that of the combined series. Note that the vertical scale is not the same for all panels.

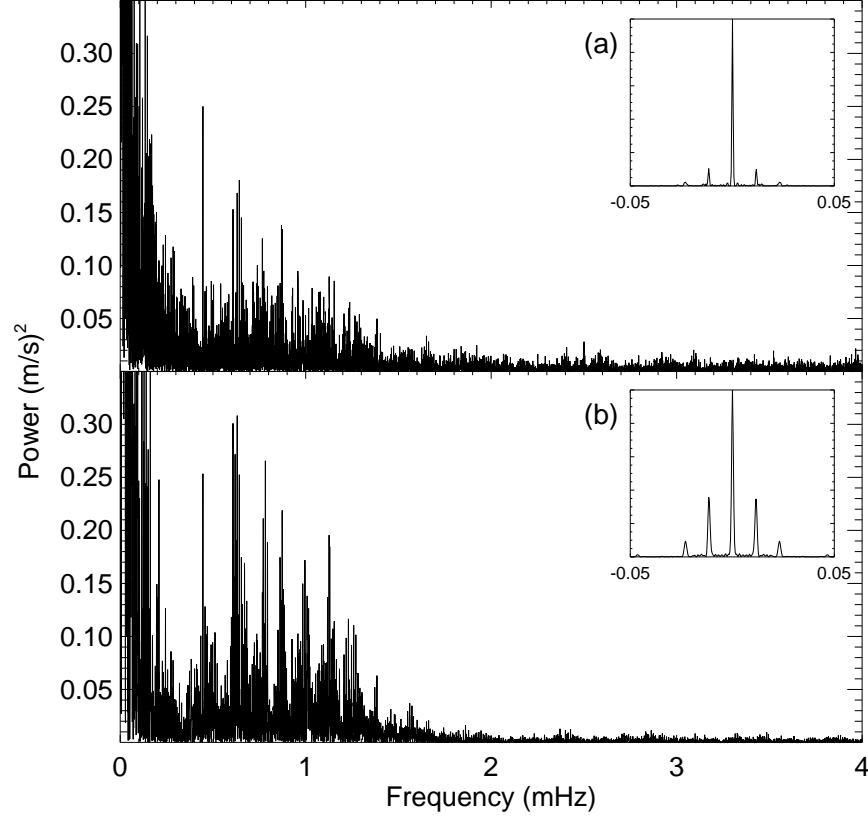


FIG. 6.— Final power spectrum based on the noise-optimized weights (lower panel), and also without applying the weights (upper panel). The inset shows the spectral window.

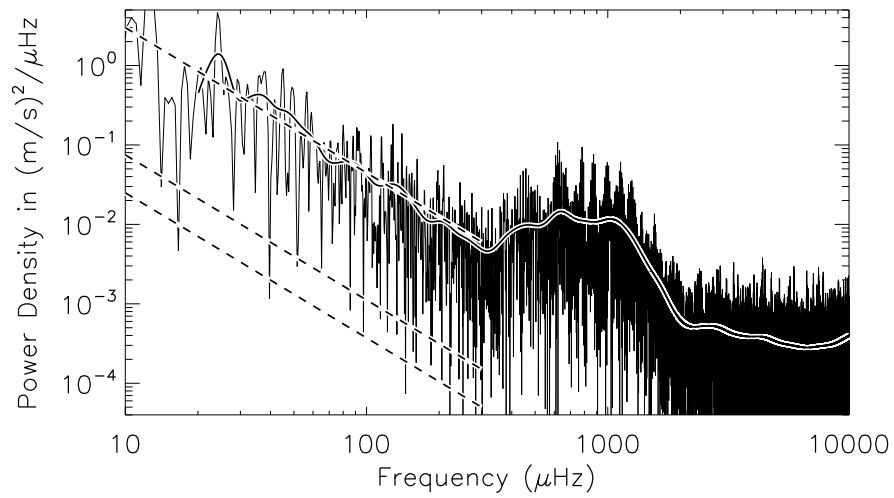


FIG. 7.— Power density spectrum of Procyon from the HARPS data, and the same after smoothing. The lower two dashed lines show the solar activity level at minimum and maximum, and the upper line is the solar maximum activity shifted upwards by a factor of 40.

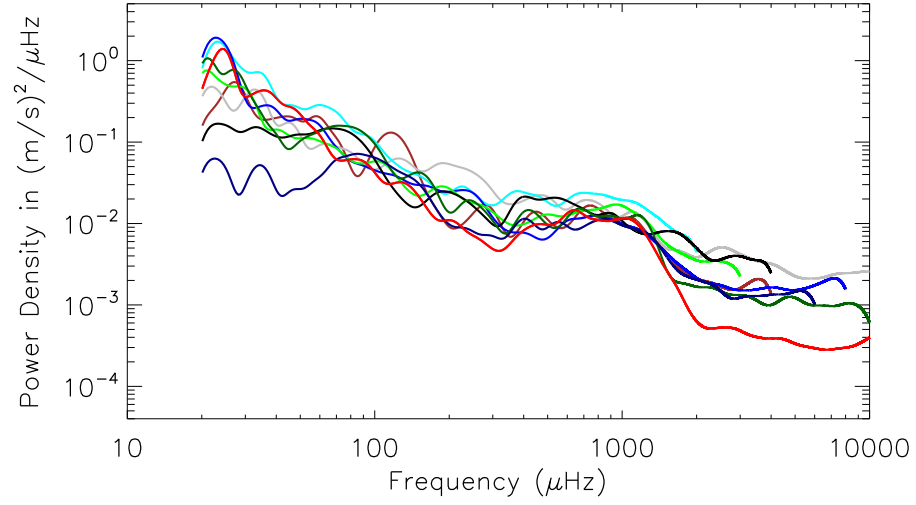


FIG. 8.— Smoothed power density spectra (see Fig 7) for the nine telescopes shown in Fig. 1*a*, showing a similar background from stellar noise at low frequencies and different levels of white noise at high frequencies. The color coding is the same as in Fig. 1.

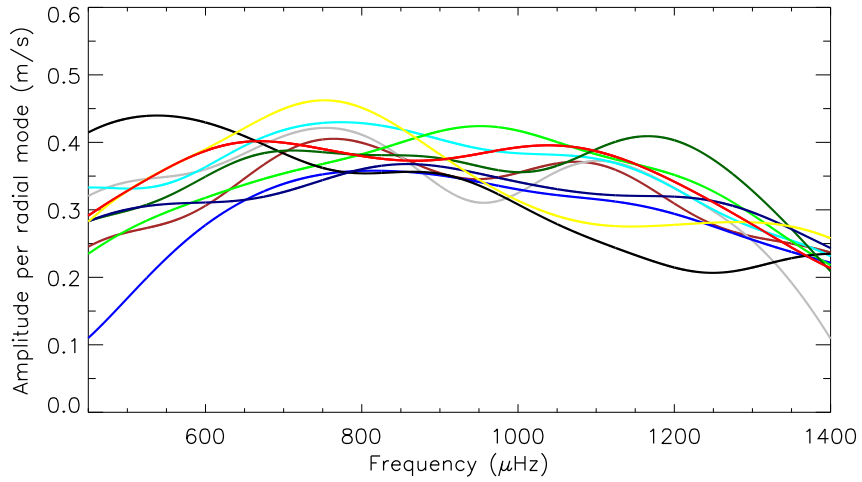


FIG. 9.— Smoothed amplitude curves for Procyon for ten telescopes, using the same color coding as Fig. 1.

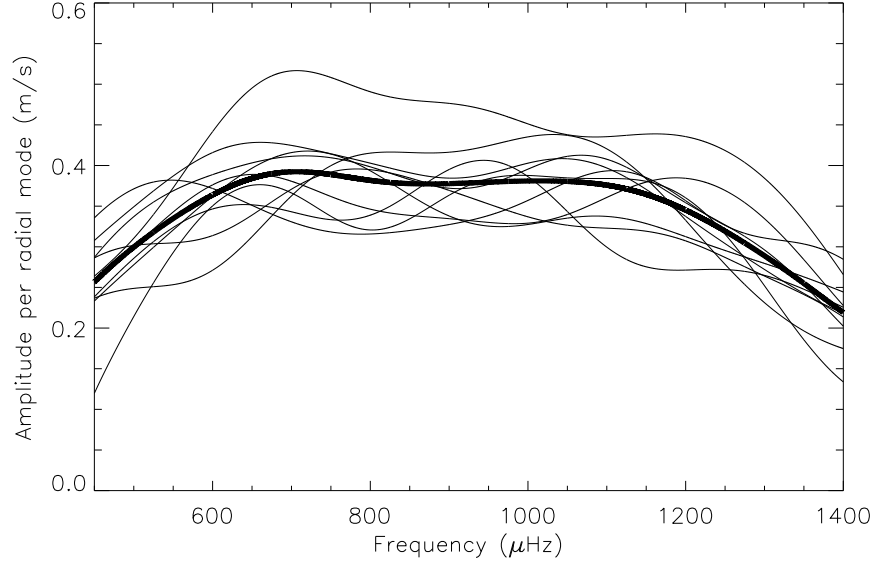


FIG. 10.— Smoothed amplitude curves for Procyon from ten 2-day segments of the combined time series (thin lines), together with their mean (thick line).

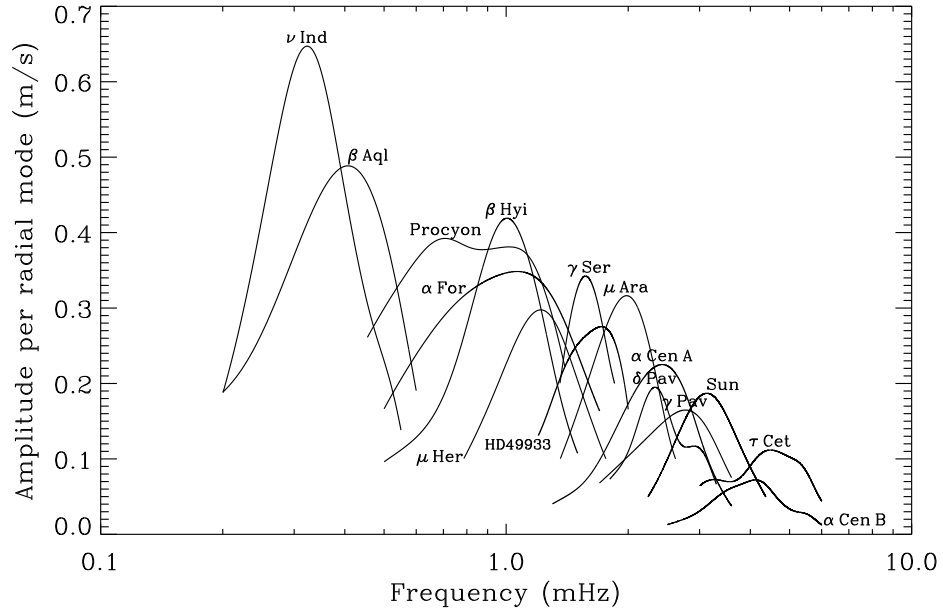


FIG. 11.— Smoothed amplitude curves for oscillations in Procyon and other stars.